Research Article

Advances in Mechanical Engineering

Advances in Mechanical Engineering
2018, Vol. 10(6) 1–13

DOI: 10.1177/1687814017734133
journals.sagepub.com/home/ade
SAGE

A numerical investigation of microwave ablation on porous liver tissue

Pornthip Keangin[1] and Phadungsak Rattanadecho[2]

Abstract

The understanding of heat transport in biological tissues is important for enhanced insight on the physiological mechanisms and thermoregulatory mechanisms. This article presents a numerical simulation of microwave (MW) ablation using a single-slot MW antenna on two layers of porous liver tissue. The two layers are of tumor and normal tissue. A porous media approach is proposed for mathematical model of MW ablation. Three coupled models which include transient momentum equations and a transient energy equation coupled with an electromagnetic wave propagation (EWP) equation are analyzed. This article focuses on the influences of the tumor diameter, tumor porosity, and input MW power on the specific absorption rate (SAR) profile, temperature profile, and blood velocity profile within the porous liver tissue. The results obtained from the calculation of porous media model are examined and compared with the one of bioheat model along with the experimental results from previous work. The results indicated that all parameters have a significant effect on the SAR profile, temperature profile, and blood velocity profile in the porous liver tissue. The advanced results in this research can be used in applications such as it provides guidance on the practical treatment and can be developed medically for therapeutic.

Keywords

Bioheat model, heat transfer, liver tissue, microwave ablation, porous media model

Date received: 15 May 2017; accepted: 30 August 2017

Handling Editor: Liyuan Sheng

Introduction

A new advancing technique for cancer treatment is microwave (MW) ablation. This is a method that transmission of heat from MW energy via the MW antenna to kill cancer cells while doing little or no damage to surrounding healthy tissues. MW ablation is a slightly invasive local treatment of tumors, especially where the tumor infiltrates deeply into the tissue, can also reduce the impact on patients due to the use of anti-cancer drugs.[1] One of its benefits is it produces a larger active heating region on the tissue, leading to considerably more effective treatment. Therefore, the topic of heat transfer in human tissue during MW ablation has been of interest for several years, especially MW ablation treatment of liver cancer. However, experimental of MW ablation therapy cannot be applied on live human beings due to ethical considerations. Experimental studies in animals are another choice for researchers[2–4]; but, some properties of animals may not be applicable in a wide range of realistic situations of cancer

[1]Department of Mechanical Engineering, Faculty of Engineering, Mahidol University, Salaya, Thailand
[2]Department of Mechanical Engineering, Faculty of Engineering, Thammasat University, Rangsit, Thailand

Corresponding author:
Phadungsak Rattanadecho, Department of Mechanical Engineering, Faculty of Engineering, Thammasat University, Rangsit Campus, 99 Moo 18, Paholyothin Road, Klong Nueng, Klong Luang, Rangsit 12120, Pathum thani, Thailand.
Email: ratphadu@engr.tu.ac.th

treatment. It is a more completely relevant process of MW ablation to improve a realistic biological tissue model via numerical simulation. Numerical analysis of tissue MW thermotherapy can provide useful information on the studied cancer treatment under a variety conditions as it is a rapid and inexpensive way to test innovative medical equipment design.

In the past, the studies of MW ablation dealt with homogeneous material and focused on heat conduction using Pennes' bioheat equation.[5] Pennes' bioheat model is widely used for modeling the heat transport of biological tissues during thermal therapy.[6–8] Also, due to the simplifications and limitations of this model, Pennes' bioheat equation is based on the assumption of all heat exchange between the tissue and vascular occurs in the capillaries[9] and assumes that the temperature of the vascular within the capillaries is equivalent to the core temperature of the human body.[10] Therefore, other researchers have developed bioheat modeling by extending, modifying, or coupling this model with other models.[11–15]

In reality, biological tissues are complex structures consisting of cells of different sizes and a microvascular bed in which the blood flow direction contains various vessels as we referred to as porous structure. Investigation of heat transfer using the anatomical structure of biological tissues can be represented more accurately via porous media theory. With only a few assumptions, porous media models have been applied to analyze the heat transfer in biological tissues in recent years. Most of previous works on the modeling of heat transport focused on single-layer porous media biomaterials.[16–18] Some studies on the modeling of the heat transport of layered materials.[19–23] Although porous media models have been used for heat transfer studies in some multilayer biomaterials in previous investigations, they did not utilize porous media modeling in representing the thermal transport of various effects, such as tumor diameter, tumor porosity, and input MW power. In practical treatment, these effects can enhance the heat transfer process of absorption within the target tissue. Therefore, in order to provide adequate information on MW ablation, it is essential to consider complete modeling based on porous media theory in multilayer porous liver tissue and consider all of the previously mentioned parameters in the analysis so as to represent the actual process of MW ablation.

This study is to investigate the influences of tumor diameter, tumor porosity, and input MW power. A mathematical model of the process through MW ablation is expressed completely by the transient momentum equations and the transient energy equation coupled with the electromagnetic wave propagation (EWP) equation to investigate the characteristics of specific absorption rate (SAR) profile, temperature profile, and blood velocity profile in two-layer porous liver with embedded tumor during MW ablation. Governing equations in the study are analyzed by the axisymmetric finite element method (FEM). The values obtained provide an indication toward understanding the realistic situation of MW ablation and serve as a first step for the development of medically safe for MW ablation treatments.

Models

For MW ablation, an MW antenna is inserted into a tumor to release MW energy (insertion depth of 70.5 mm). The goal of MW ablation is to raise the temperature of the unwanted tissue (tumor) to 50°C or above, at which cancer cells are destroyed.[24] In this research, a single-slot MW antenna is situated into the porous liver tissue to deliver input MW power in order to destroy the tumor. The single-slot MW antenna with a diameter of 1.79 mm is applied because this thin antenna is need in interstitial MW therapy to affect the tissues of the body minimally. The dimension of the ring-shaped slot is 1 mm wide and is cut off from the outer conductor of 5.5 mm in length from the short circuited tip to effectively treat deep-seated tumors. The effective heating is formed at locations around the antenna tip and is very significant for effective interstitial hyperthermia.[25] The single-slot MW antenna has three components: inner conductor, dielectric, and outer conductor. For hygienic and guidance purposes, the antenna is enclosed in a catheter which made of polytetrafluoroethylene (PTFE). Figure 1 displays the geometry of a single-slot MW antenna. The working frequency of the antenna is 2.45 GHz, a widely used frequency in MW ablation. The dimensions of the single-slot MW antenna are shown in Table 1, while its dielectric properties are listed in Table 2.

Figure 2 depicts the computational domain of the problem. The porous liver tissue comprises of two

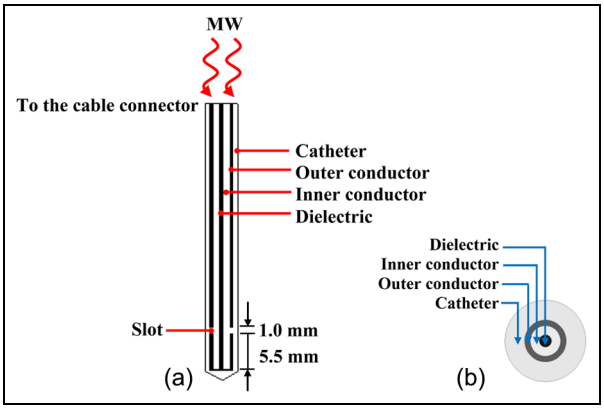

Figure 1. Model geometry of a single-slot MW antenna: (a) schematic of a single-slot MW antenna and (b) cross section of a single-slot MW antenna.

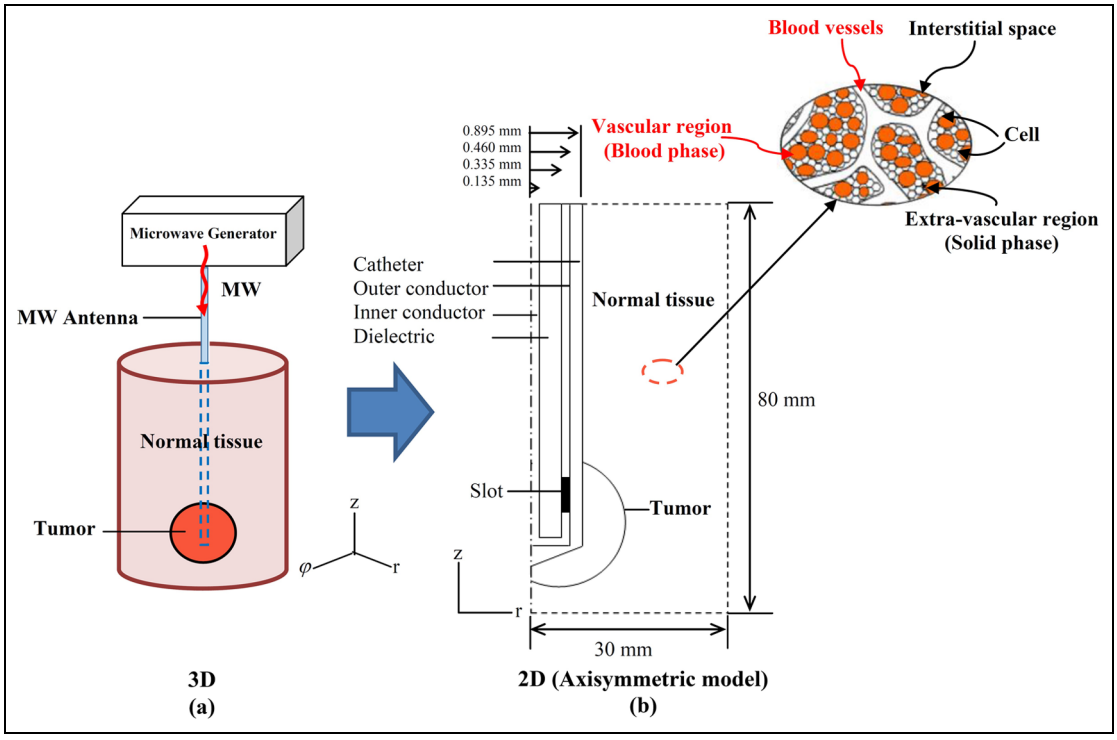

Figure 2. Physical model: (a) 3D porous media model and (b) 2D axisymmetric model.

Table 1. Dimensions of a single-slot MW antenna.

Materials	Dimensions (mm)
Inner conductor	0.135 (radial)
Dielectric	0.335 (radial)
Outer conductor	0.460 (radial)
Catheter	0.895 (radial)
Slot	1.000 (wide)

Table 2. The dielectric properties of a single-slot MW antenna.

Properties	Value		
	Dielectric	Catheter	Slot
Relative permittivity ε_r (–)	2.03	2.1	1
Electric conductivity σ (S/m)	0	0	0
Relative permeability μ_r (–)	1	1	1

parts, that is, the tumor and normal tissue. A cylindrical geometry of porous liver tissue with a radius of 30 mm and a height of 80 mm is considered. The anatomical structure of the porous liver tissue is assumed to have spaces between cells which are filled with blood (blood-saturated porous media). Within a cylindrical geometry of porous liver tissue, we consider a tumor in spherical shape with different diameters. The approach based on assuming a spherical and cylindrical geometry for the tumor and normal tissue, respectively, has been used in several works.[20,23,26,27]

In an anatomical structure, the biological tissues comprise of three components which are blood vessels, cells, and interstitial space. However, most previous studies have categorized into two distinct regions, that is, the vascular region (blood vessels) and the extra-vascular region (cells and the interstitial space), and the whole anatomical structure can be treated as a blood-saturated tissue represented by a porous matrix in which the blood infiltrates through.[16,17,20,23] The vascular region refers to as a blood phase and a solid matrix phase is regarded as an extra-vascular region, as explained in Figure 2.

Problem formulation

EWP analysis

The EWP model is calculated using Maxwell's equations. The general form of Maxwell's equations based on the harmonic propagation assumption is simplified to demonstrate the SAR profile. This research is carried out with the following assumptions:

1. The EWP is rendered in two-dimensional (2D) axially symmetric cylindrical coordinates (r–z).[28]

2. An electromagnetic wave propagates along the single-slot MW antenna, is characterized by transverse electromagnetic (TEM) field.[29]
3. A transverse magnetic (TM) field is used to characterize an electromagnetic wave in the porous liver tissue.[29]
4. The wall of the single-slot MW antenna is assumed to be a perfect electric conductor (PEC).
5. The outer surface of the porous liver tissue is shortened by a scattering boundary condition (the electromagnetic wave can pass through the boundary without reflection) and the electromagnetic wave is confined to the porous liver tissue.

In this work, the adapted axisymmetric finite element (FE) model is utilized.[13,20,28] The electric and magnetic fields associated with the time-varying TEM wave is analyzed in 2D axially symmetric cylindrical coordinates

$$\text{Electric field } (\vec{E}) \quad \vec{E} = e_r \frac{C}{r} e^{j(\omega t - kz)} \tag{1}$$

$$\text{Magnetic field } (\vec{H}) \quad \vec{H} = e_\phi \frac{C}{rZ} e^{j(\omega t - kz)} \tag{2}$$

where

$$C = \sqrt{\frac{ZP}{\pi \cdot \ln(r_{outer}/r_{inner})}} \tag{3}$$

Z is the wave impedance (Ω), P is the input MW power (W), while r_{inner} and r_{outer} are the dielectric's inner and outer radius (m), respectively. Furthermore, $\omega = 2\pi f$ denotes the angular frequency (rad/s) where f is the frequency (Hz). $k = 2\pi/\lambda$ represents the propagation constant (m^{-1}) and λ is the wave length (m).

In the porous liver tissue, the electric field has an axial component, whereas the magnetic field is purely in the azimuth direction.[29] In the coaxial cable the electric field is considered only in the radial direction. However, there is considered both in the radial and the axial directions inside the tissue. This assumption encourages the single-slot MW antenna to be modeled using an axisymmetric TM wave formulation and based on harmonic propagation. The wave equation is simplified for $\vec{H}_\varphi$ as follows

$$\nabla \times \left(\left(\varepsilon_r - \frac{j\sigma}{\omega \varepsilon_0} \right)^{-1} \nabla \times \vec{H}_\phi \right) - \mu_r {\gamma_0}^2 \vec{H}_\phi = 0 \tag{4}$$

where ε_0 is the permittivity of vacuum/free space and is equal to 8.8542×10^{-12} F/m, ε_r is the relative permittivity (−), σ is the electric conductivity (S/m), μ_r is the relative permeability (−), and γ_0 is the free space wave number (m^{-1}).

Boundary condition for EWP analysis

The single-slot MW antenna is connected to the MW generator and is placed into the porous liver tissue. MW energy which is generated by MW generator propagates in single-slot MW antenna into the porous liver tissue from the slot to destroy cancerous tissue. The boundary conditions for determining EWP is considered as follows.

At the inlet of the single-slot MW antenna, TM wave propagation with various input MW powers is assigned. At $r = 0$, an axis symmetry boundary condition is used

$$\vec{E}_r = 0 \tag{5}$$

$$\frac{\partial \vec{E}_z}{\partial r} = 0 \tag{6}$$

The scattering boundary conditions (waves can be pass through boundary without reflection) for $\vec{H}_\varphi$ are used along the outer sides of the porous liver tissue boundaries

$$\hat{n} \times \sqrt{\varepsilon}\vec{E} - \sqrt{\mu}\vec{H}_\phi = -2\sqrt{\mu}\vec{H}_{\phi 0} \tag{7}$$

where $\vec{H}_{\phi 0} = C/Zr$ is the excitation magnetic field.

The inner and outer conductors of the single-slot MW antenna are modeled as the PEC boundary conditions

$$\hat{n} \times \vec{E} = 0 \tag{8}$$

The continuity boundary condition is applied for electric field at the boundary between normal tissue and tumor

$$\hat{n} \times (\vec{E}_n - \vec{E}_t) = 0 \tag{9}$$

Blood flow and heat transfer analysis

Solving the governing equations for the blood velocity and temperature profiles in the porous liver tissue has been evaluated by the transient momentum equations via Brinkman extended Darcy model and transient energy equation, respectively. This research is carried out on the blood flow and the heat transfer examination which is based upon the following assumptions:

1. Corresponding to the EWP analysis, the blood flow and heat transfer analysis in the porous liver tissue is modeled to be in 2D axially symmetric cylindrical coordinates (r–z).
2. The porous liver tissue is homogeneous, thermally isotropic, and blood-saturated material.[20]
3. The incompressible Navier–Stokes model is used to simulate the laminar flow conditions in the blood vessel.[30]

4. The local thermal equilibrium (LTE) heat transfer between solid and blood phases is considered.
5. The energy exchange across the outer surface of the porous liver tissue is negligible, and nor phase change and nor chemical reactions occur in the porous liver tissue.
6. The effect of buoyancy due to the temperature gradient is modeled using the Boussinesq approximation.[31,32]

Momentum equations. In the present numerical work, the Brinkman extended Darcy flow model is used for studying the blood flow within the porous liver tissue, which was first described by Brinkman.[33] The governing equations for explaining the blood flow within porous liver tissue are as follows[20]

Continuity equation

$$\frac{\partial u}{\partial r} + \frac{\partial w}{\partial z} = 0 \tag{10}$$

Momentum equations

$$\frac{1}{\varphi}\left(\frac{\partial u}{\partial t}\right) + \frac{1}{\varphi^2}\left(u\frac{\partial u}{\partial r} + w\frac{\partial u}{\partial z}\right) = -\frac{1}{\rho_b}\left(\frac{\partial p}{\partial r}\right) + \frac{\nu}{\varphi}\left(\frac{\partial^2 u}{\partial r^2} + \frac{\partial^2 u}{\partial z^2}\right) - \frac{u\nu}{\kappa} \tag{11a}$$

$$\frac{1}{\varphi}\left(\frac{\partial w}{\partial t}\right) + \frac{1}{\varphi^2}\left(u\frac{\partial w}{\partial r} + w\frac{\partial w}{\partial z}\right) = -\frac{1}{\rho_b}\left(\frac{\partial p}{\partial z}\right) + \frac{\nu}{\varphi}\left(\frac{\partial^2 w}{\partial r^2} + \frac{\partial^2 w}{\partial z^2}\right) - \frac{w\nu}{\kappa} + g\beta(T - T_\infty) \tag{11b}$$

From equation (11), the first term on the right hand side is the pressure gradient term, the second viscous term is the Darcy term and the third term is the analogous to the momentum diffusion term in the Navier–Stokes equation to simulate the laminar flow conditions in a blood vessel.[30] Where u and w are the blood velocity component (m/s) ($\vec{u} = (u, w)$), ϕ is the porosity which is the ratio of the vascular space volume to the tissue volume, p is the pressure (Pa), $\nu = 3.78 \times 10^{-7}$ m^2/s is the kinematics viscosity, $\beta = 1 \times 10^{-4}$ 1/K is the coefficient of the thermal expansion, and κ is the permeability (m^2).

However, the blood velocity and temperature in this work is very little, and therefore, the density varies little, yet the buoyancy drives the motion. Thus, the variation in density is neglected everywhere except in the buoyancy term. The viscous boundary layer in the porous medium is essential for heat transfer calculations, even though it is very thin.[34] Furthermore, the inertial result is also neglected since the flow is very little.

Energy equation. The energy equation assumes that the temperature of solid and blood phases are identical (LTE model) where the MW energy is included as given by Rattanadecho and Keangin[20]

$$\left(\rho c_p\right)_{eff}\frac{\partial T}{\partial t} + \left(\rho c_p\right)_b\left(u\frac{\partial T}{\partial r} + w\frac{\partial T}{\partial z}\right) = K_{eff}\left(\frac{\partial^2 T}{\partial r^2} + \frac{\partial^2 T}{\partial z^2}\right) + Q_{met} + Q_{ext} \tag{12}$$

$$\left(\rho c_p\right)_{eff} = (1-\varphi)\left(\rho c_p\right)_s + \varphi\left(\rho c_p\right)_b \text{ and } K_{eff} = (1-\varphi)K_s + \varphi K_b \tag{13}$$

Two parameters in equation (13) are the overall heat capacity per unit volume and overall thermal conductivity, respectively. Subscripts *eff*, *s*, and *b* represent the effective value, solid, and blood phases, respectively. T, ρ, c_p, and K denote the average temperature (°C), density (kg/m^3), specific heat capacity (J/kg·°C), and thermal conductivity (W/m·°C), respectively.

The metabolic heat generation (Q_{met}) of 33,800 W/m^3 is determined[35] and is considered due to the circulation of blood.[36] The resistive heat generated by electric field is denoted by external heat source (Q_{ext}) as follows

$$Q_{ext} = \frac{\sigma\left|\vec{E}\right|^2}{2} \tag{14}$$

The temperature increases are strongly affected by electromagnetic fields. The SAR parameter represents the energy rate per unit mass of tissue (W/kg) which is absorbed by the biological tissues when exposed to electromagnetic fields can be expressed as

$$\text{SAR} = \frac{\sigma\left|\vec{E}\right|^2}{2\rho} \text{ or } \text{SAR} = \frac{Q_{ext}}{\rho} \tag{15}$$

Boundary condition for blood flow and heat transfer analysis

The blood flow and heat transfer problem are analyzed only in the porous liver tissue except the single-slot MW antenna. The boundaries of porous liver tissue correspond to the hypothesis are determined in the following.

An axis symmetry boundary condition is applied at $r = 0$ for the blood flow and heat transfer analysis

$$\hat{n}\cdot\vec{u} = 0 \tag{16}$$

$$\hat{n}\cdot\left(-pI + \left(\frac{1}{\varphi}\right)\eta\left(\nabla\cdot\vec{u} + \left(\nabla\cdot\vec{u}\right)^T\right)\right) = 0 \tag{17}$$

$$\hat{n}\cdot\left(K_{eff}\nabla T - \left(\rho c_p\right)_b\vec{u}T\right) = 0 \tag{18}$$

The surroundings of the porous liver tissue are keeping at body temperature (37°C) and the boundaries for blood flow analysis are considered an open boundary condition

$$\hat{n} \cdot \left(-pI + \left(\frac{1}{\varphi} \right) \eta \left(\nabla \cdot \vec{u} + \left(\nabla \cdot \vec{u} \right)^T \right) \right) = -F_0 \cdot \hat{n} \quad (19)$$

where η is the dynamic viscosity (Pa·s) and F_0 is the normal stress (N/m^2).

The outer surface between the single-slot MW antenna and the porous liver tissue is considered as adiabatic boundary condition

$$\hat{n} \cdot \left(K_{eff} \nabla T \right) = 0 \quad (20)$$

The interaction surface between single-slot MW antenna and porous liver tissue is assumed to be rigid body motion as well as no-slip boundary conditions

$$\vec{u} = 0 \quad (21)$$

The internal boundary along the interfaces between normal tissue and the tumor is identified as continuity boundary conditions (no contact resistant occurs)

$$\begin{aligned} \hat{n} \cdot \Bigg(& -p_t I + \eta_t \left(\nabla \cdot \vec{u}_t + \left(\nabla \cdot \vec{u}_t \right)^T \right) \\ & + p_n I - \eta_n \left(\nabla \cdot \vec{u}_n + \left(\nabla \cdot \vec{u}_n \right)^T \right) \Bigg) = 0 \end{aligned} \quad (22)$$

$$\hat{n} \cdot \left(K_{eff} \nabla T_t - \left(\rho c_p \right)_b \vec{u} T_t - K_{eff} \nabla T_n - \left(\rho c_p \right)_b \vec{u} T_n \right) = 0 \quad (23)$$

The initial temperature within the porous liver tissue is considered as a constant core body temperature at 37°C. Numerical modeling is utilized to perform the FEM via COMSOL™ Multiphysics to analyze the problems. The axisymmetric FE model is performed. The number of elements that the solution to the numerical model is independent of the mesh density is approximately 20,471 elements. We assume that the dielectric and thermal properties and porosities of porous medium are constant. Table 3 tabulates the dielectric and thermal properties of porous medium used in the computations.

Table 3. The dielectric and thermal properties of normal tissue, blood, and tumor.[29,37–39]

Properties	Value		
	Normal tissue (*n*)	Blood (*b*)	Tumor (*t*)
Relative permittivity; ε_r (–)	43	58.3	48.16
Electric conductivity; σ (S/m)	1.69	2.54	2.096
Density; ρ (kg/m^3)	1,030	1,058	1,040
Specific heat capacity; c_p (J/kg °C)	3,600	3,960	3,960
Thermal conductivity; K (W/m°C)	0.497	0.45	0.57

Results and discussion

Verification of the model

The accuracy of this work is verified by the validation against the results offered by Yang et al.[12] by selection of an input MW power of 75 W with a frequency of 2.45 GHz and the initial liver tissue temperature of 8°C. The axisymmetric model is considered to analyze the MW ablation system. The validation results are illustrated in Figure 3 for the distribution of temperature in the liver tissue for 50 s, which it is considered at positions of 4.5 and 9.5 mm away from the single-slot MW antenna. Figure 3(a) depicts the validation results of the liver tissue temperature of the presented bioheat model compared with the liver tissue temperature of the bioheat model obtained by Yang et al.[12] It produces similar results with Yang et al.[12] In addition, to verify the accuracy of the presented model of MW ablation, the resulting data of the bioheat and porous media models are verified with the experimental data presented by Yang et al.[12] under the same geometric model and same conditions. The comparison of results is depicted in Figure 3(b); it is seen that the simulation results are in agreement with the experimental data. In addition, the simulation results obtained from porous media model follow closer to the experimental results than the one from bioheat model. At the same range of time of both positions, their temperature distributions provide similar results. This is because the heat transfers in the porous media model are governed both by conduction and convection modes. In contrast, the bioheat model is mainly generated by the conduction heat mode. Therefore, it is reasonable to select the porous media modeling approach which can be effectively used for this problem. This comparison guarantees that the numerical model can accurately represent the transport phenomena in the liver tissue. This is important to achieve near-realistic model of the MW ablation problem.

In this study, the influences of the three parameters, namely, the tumor diameter (D = 1.4, 2.0, and 2.6 cm), the tumor porosity (ϕ_t = 0.4, 0.5, 0.6, and 0.7), and the input MW power (P = 10, 15, and 20 W), have been investigated. A parametric study has been performed to estimate the effects of each of these variables, separately, and analyze their contributions in determining the SAR, temperature, and blood velocity profiles.

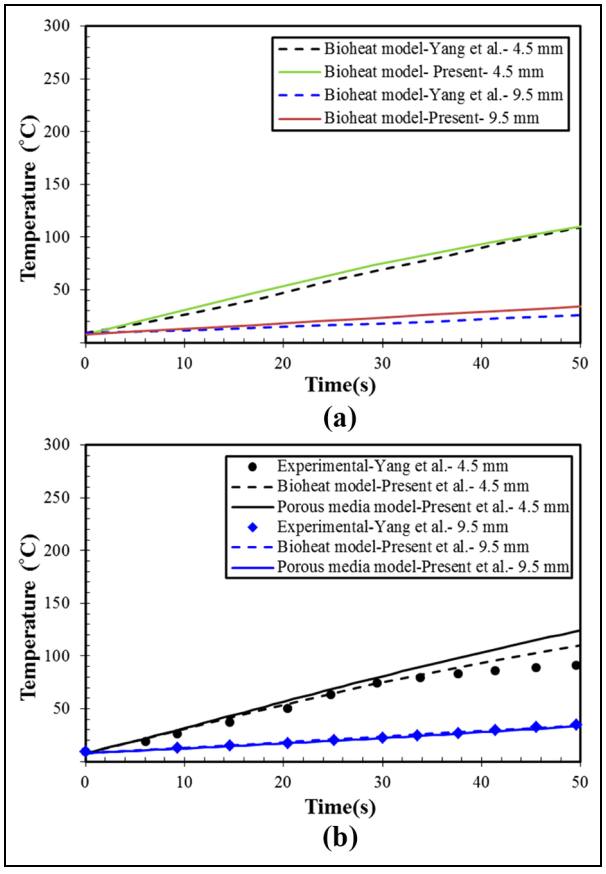

Figure 3. Validation of the mathematical model against Yang et al.:[12] (a) validation results of the liver tissue temperature of bioheat model and (b) validation results of the liver tissue temperature of bioheat model and porous media model to experimental data.

Comparison of bioheat model and porous media model

Comparative studies on the transport of heat transfer using the bioheat and porous media models are performed and evaluated in detail to support the results stated within this article. The resulting transient temperature profile in liver tissue for durations of 0–300 s based on $P = 10$ W, $f = 2.45$ GHz, and $D = 2.0$ cm for the bioheat and porous media models is shown in Figure 4. It is found that the temperature profiles in both models are very similar at a particular time but slightly different magnitudes. In both models, the temperature profile forms a nearly oval shape around the slot. The areas with highest temperature value (hot spot zone) occur in the vicinity of the slot of the single-slot MW antenna. This happens because the blood flow in the void of the porous media model is often very slow and therefore has a small effect on the temperature profile within the porous liver tissue. The reason why the present model is preferable to use in this problem, the porous media model can also show the blood velocity profile, which is the result of effects of density variation due to thermal gradients. The blood circulation presented in this article could possibly occur in a realistic situation due to its very high temperature and high energy density in the MW ablation process.

Tumor diameter effect

The effect of tumor diameter on the SAR profile within the porous liver tissue at $P = 10$ W, $f = 2.45$ GHz, $\phi_n = 0.6$, $\phi_t = 0.7$, and $t = 300$ s are shown in Figure 5. Figure 5(a)–(c) show the SAR profile of the porous liver tissue at the tumor diameters of 1.4, 2.0, and 2.6 cm, respectively. These figures illustrate the volumetric heating effect expected from MW ablation, where a hot spot zone occurs at the position near the end tip and the slot of the single-slot MW antenna. The calculated results for SAR profile are consistent closely with the experimental SAR profile in the research of Deshazer et al.[40] MW power delivered from the antenna propagates inside the tumor and the normal tissue and is transformed into the thermal energy by electromagnetic heating. The SAR profile curves form a nearly oval distribution around the slot and it has the highest value near the antenna slot for all tumor diameters. It then reduces by distance, leading to a higher value of SAR in the tumor than the normal tissue. Nevertheless, the volumetric SAR pattern within the porous liver tissue in the case of a greater tumor diameter provides a broader area of heat dissipation to the surrounding tissue near the slot of the antenna compared with result calculated for a smaller tumor diameter.

Figure 6(a)–(c) show the effect of the tumor diameter on the temperature profile within the porous liver for tumor diameters of 1.4, 2.0, and 2.6 cm, respectively. This figures show that the temperature profile follows the SAR profile quite well. The higher temperature value location corresponding to the higher SAR value in that area. The increase of temperature in the porous liver tissue happens because the absorption of the MW power as well as SAR within the porous liver tissue, and thereafter, the absorbed energy is converted to thermal energy. The simulated temperature profiles are comparable with the experimental temperature profiles in the research of Deshazer et al.[40] The results obtained demonstrate that the maximum temperature value is above 50°C in tumor region, which is capable of destroying tumor in the liver tissue (usually, tumors are destroyed at temperatures over 50°C[24]). However, in the case of a tumor diameter of 1.4 cm, it is established that the area surrounding the tumor region has a temperature exceeds 50°C that will damage the normal tissue around the tumor region. It is found that the smaller tumor diameter gives a slightly higher temperature value within the porous liver tissue.

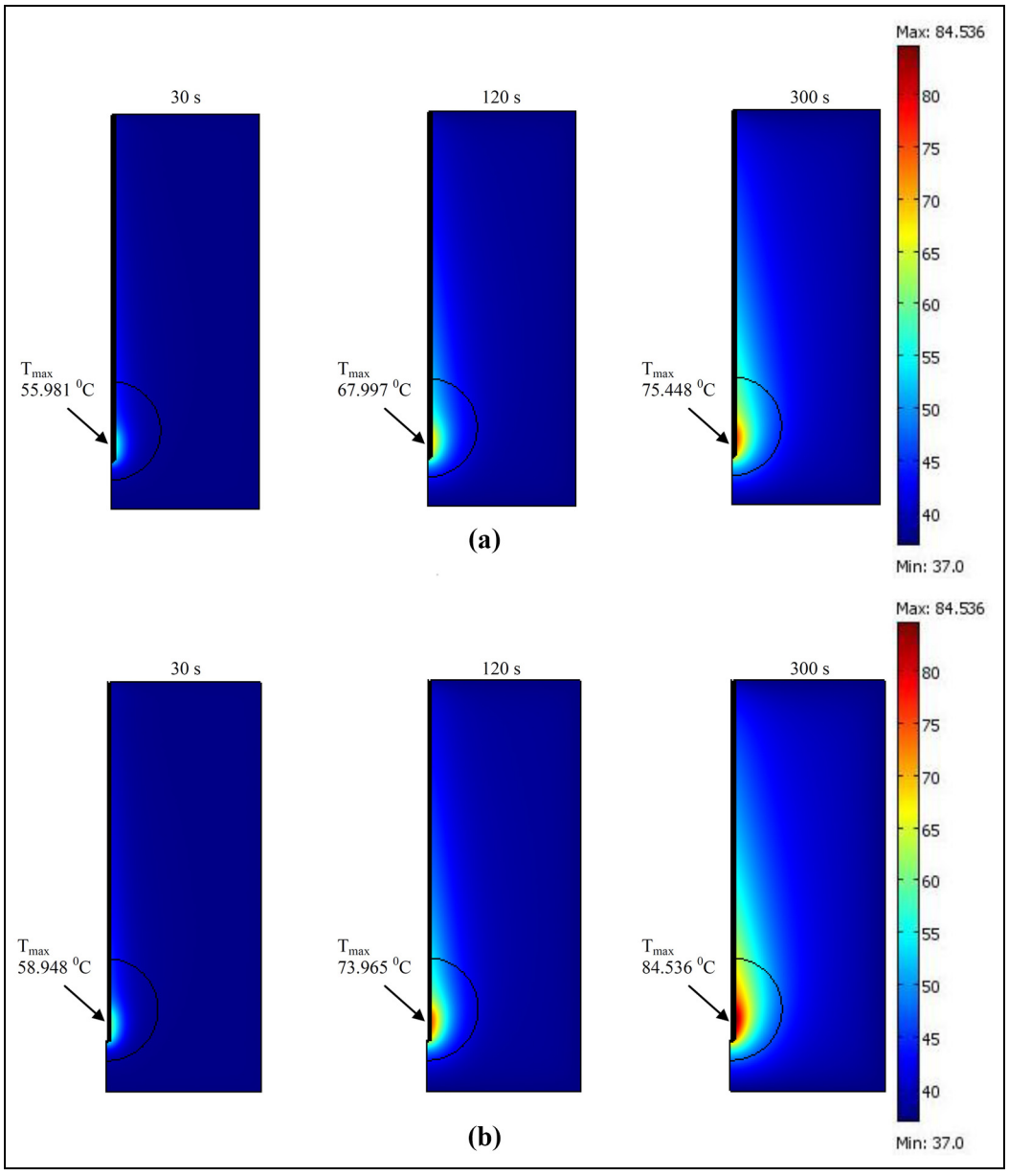

Figure 4. Simulated temperature profiles at various times based on P = 10 W, f = 2.45 GHz, and D = 2.0 cm for (a) bioheat model and (b) porous media model.

Furthermore, the greater tumor diameter provides a wider region of heat far away from the antenna because of the effect of natural convection through the pores of the tumor on heat transfer. The natural convection due to blood circulation is confirmed as illustrated in Figure 7. Figure 7(a)–(c) show the blood velocity profile of the porous liver tissue with the following conditions in the previous figures at tumor diameters of 1.4, 2.0, and 2.6 cm, respectively. The blood flows are driven by the effect of buoyancy force (natural convection) due to MW energy. The blood flow with higher velocity act as a heat sink by dissipating the heat to the surrounding tissue. The warmer blood upward toward the top and contributes to the convection cooling effect near the vicinity of the antenna slot, while far from the antenna, the heat source is weaker leads to lower temperatures and colder blood with lower velocity. It is shown that the normal tissue receives weakened MW energy with lower porosity and a lower permeability, causing the blood velocity within this normal tissue to be very weak. Considering the effect of the tumor diameter on the blood velocity, the smaller diameter yields a slightly lower blood velocity compared to that of the greater tumor diameter due to the weakness of the natural convection.

Figure 8(a)–(c) show the effect of tumor diameter on the SAR distribution, the temperature distribution, and

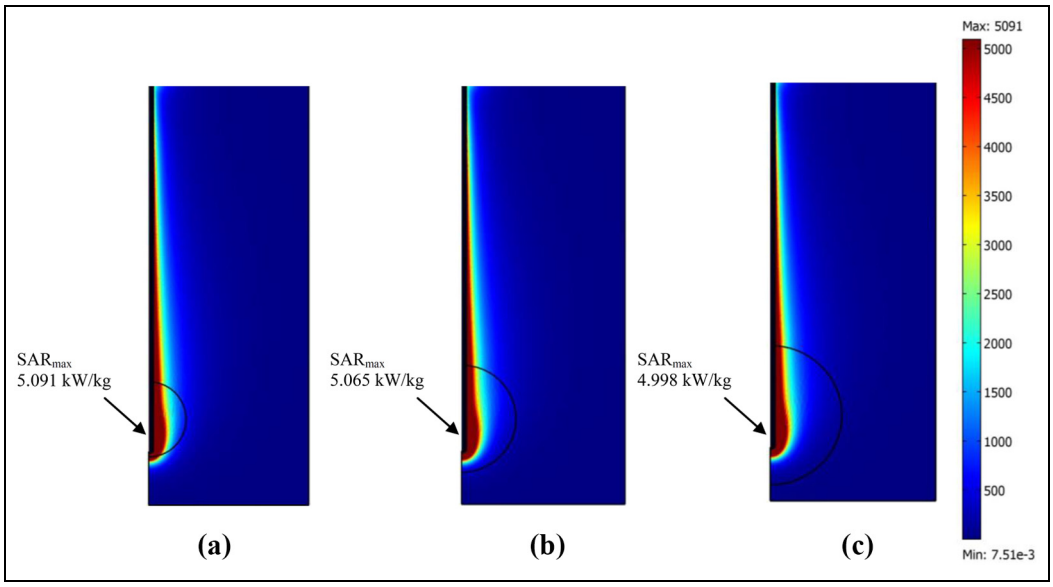

Figure 5. The SAR profile in the porous liver tissue at various tumor diameters for (a) D = 1.4 cm, (b) D = 2.0 cm, and (c) D = 2.6 cm.

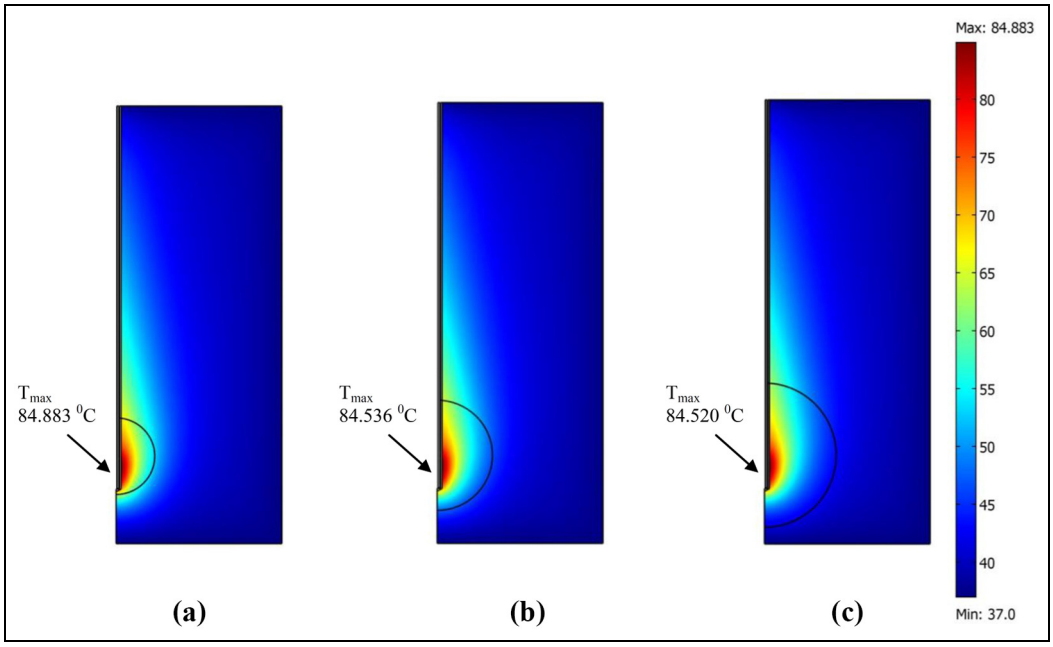

Figure 6. The temperature profile in the porous liver tissue at various tumor diameters for (a) D = 1.4 cm, (b) D = 2.0 cm, and (c) D = 2.6 cm.

the blood velocity distribution along the path guidance (z = 16 mm or insertion depth of 64 mm), respectively. From Figure 8(a), it can be observed that the maximum of SAR value slightly changes according to tumor diameter. The SAR distributions gradually increase through the path guidance and quickly decrease and have the lowest value with r = 30 mm. Figure 8(b) shows that the distributions of temperatures are same pattern but are a little different in magnitude for each diameter. The temperature rapidly increases along the path guidance and to a highly temperature localized near the slot of the antenna and then decreases continuously along the distance and approaches 37°C due to the penetration depth which relates to the SAR distribution. It is interesting to observe that the hot spot zone happens in the tumor meaning that the temperature in the tumor is higher than the temperature in the normal tissue. However, the tumor diameter has only a small

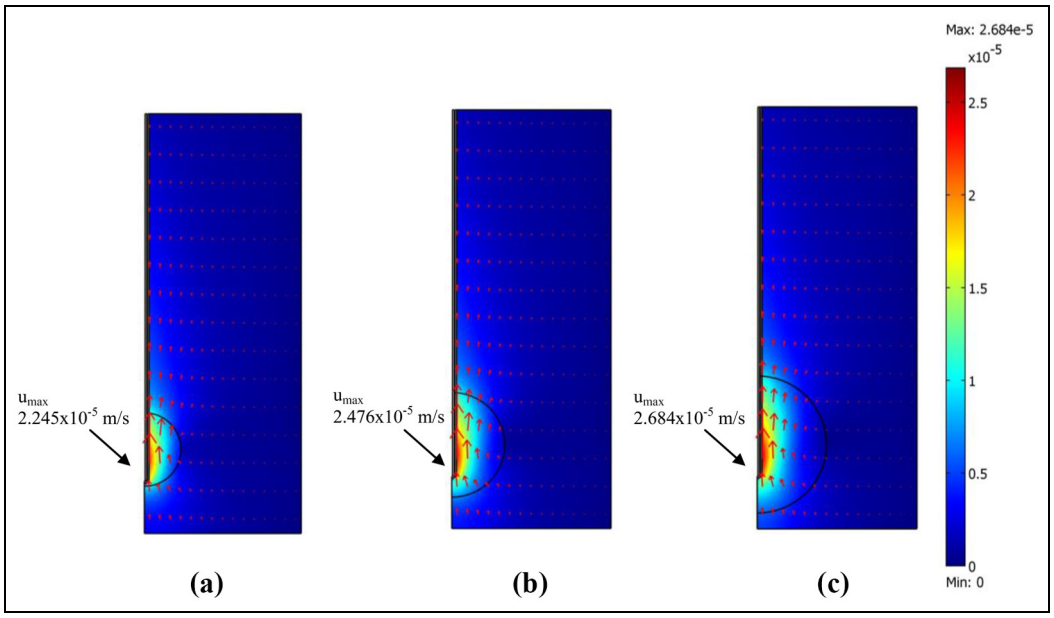

Figure 7. The blood velocity profile in the porous liver tissue at various tumor diameters for (a) D = 1.4 cm, (b) D = 2.0 cm, and (c) D = 2.6 cm.

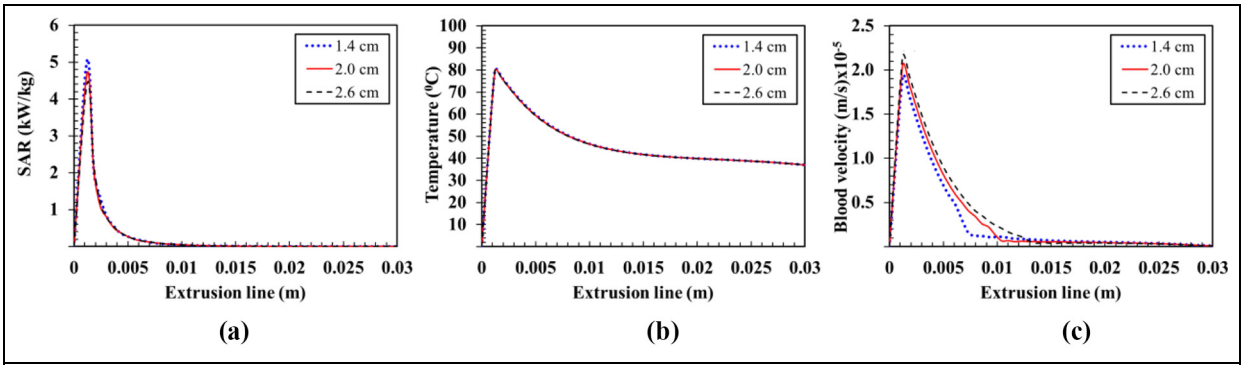

Figure 8. The effect of tumor diameter on (a) the SAR distribution, (b) the temperature distribution, and (c) the blood velocity distribution along the path guidance.

effect on the temperature distribution within the porous liver tissue, although it has a strong effect on the blood velocity distribution, as shown in Figure 8(c). The convective heat transfer characteristic has a strong effect on the blood velocity distribution. The blood velocity rapidly increases along the path guidance and reaches its maximum value near the slot of the antenna. It then the blood velocity slowly decreases and approaches zero to the outer boundaries of the porous liver tissue because it is not influenced by transmission of waves.

Tumor porosity effect

Figure 9(a) and (b) show the effect of tumor porosity on the temperature distribution and the blood velocity distribution along the path guidance. The physical data are $P = 10$ W, $f = 2.45$ GHz, $\phi_n = 0.6$, $D = 2.0$ cm, and $t = 300$ s. It is found that the temperature distributions for all porosities have the same pattern but differ slightly in magnitude. Greater tumor porosity provides greater permeability that leads to a slightly higher temperature. It is also found that the greater tumor porosity corresponds to greater blood velocity because the greater tumor porosity has a large temperature gradient produced by the MW power, causing a strong impact of natural convection that gives a buffer characteristic to the porous liver tissue temperature during the MW ablation system. The blood velocity rapidly increases along the path guidance and reaches its maximum value near the antenna slot and then gradually decreases and

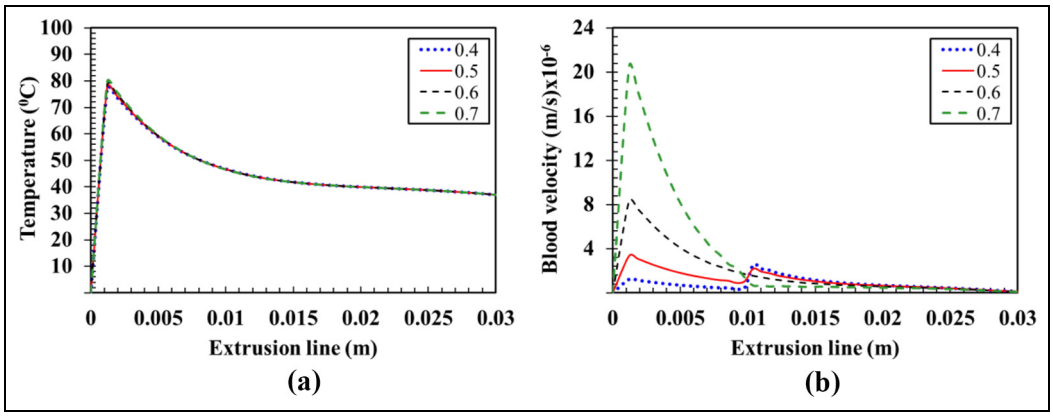

Figure 9. The effect of tumor porosity on (a) the temperature distribution and (b) the blood velocity distribution along the path guidance.

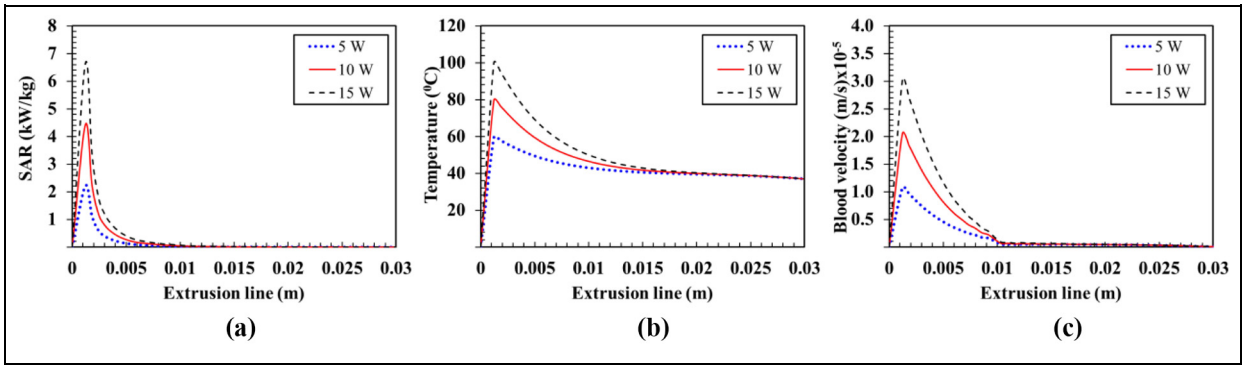

Figure 10. The effect of input MW power on (a) the SAR distribution, (b) the temperature distribution, and (c) the blood velocity distribution along the path guidance.

closer to zero at the outer boundaries of the porous liver tissue due to its not influenced by the transmission of waves in case of tumor porosities of 0.6 and 0.7. This is because the tumor is closer to the end tip and the slot of the single-slot MW antenna, so the higher porosity and higher permeability than normal tissue mean that it will receive a strong incident wave and the blood velocity within the tumor is very strong. By contrast, the normal tissue receives weakened MW energy and its lower porosity and lower permeability mean that the blood velocity within this normal tissue is very weak. However, in the case of a tumor porosity of 0.7, at the outer region between the tumor and the normal tissue, there is a small swing in the blood velocity due to the difference in the porosity of the tumor and the normal tissue. On the other hand, in the case of tumor porosities of 0.4 and 0.5, the blood velocity at $r = 0.01$ m is increased and reaches its maximum value again and then gradually decreases and approaches zero. Since the tumor has a lower porosity and a lower permeability than normal tissue, weakened MW energy will be absorbed, meaning that the blood velocity is very weak. In addition, in the case of the tumor porosities of 0.4 and 0.5, when the permeability of the tumor is low, the convective heat transfer mechanism is almost completely inhibited, that is, conduction plays a major role in heat transfer.

Input MW power effect

Figure 10(a)–(c) show the effect of the input MW power on the SAR distribution, temperature distribution, and blood velocity distribution along the path guidance based on $\phi_n = 0.6$, $\phi_t = 0.7$, $D = 2.0$ cm, $f = 2.45$ GHz, and $t = 300$ s. Once again, the findings revealed that the temperature distribution relates to the SAR distribution. The maximum temperature at the higher input MW power is clearly greater than that of the lower input MW power following SAR. Greater input MW power, leading to a higher strength of electric field, provides greater heat generation within the porous liver tissue, thereby increasing the maximum temperature during the MW ablation process. The blood velocity distributions have similar trend with the

temperature distributions which produce convective heat transfer. Greater input MW power corresponds to greater blood velocity within the porous liver tissue. The explanation of the blood flow pattern is discussed in the previous topic, where the key factor affecting the velocity of blood in the porous liver tissue is the permeability of the layers of the tumor and normal tissue.

Conclusion

Computer simulation is necessary to improve the MW ablation procedure. A method that leads to accurately lesion size control is needed for the clinical treatment with MW ablation in order to guarantee destruction of the cancer tissue and minimizing damage to surrounding healthy tissue. This research is carried out to observe the effects of tumor diameter, tumor porosity and input MW power on the SAR, temperature, and blood velocity profiles in two-layer porous liver tissue during MW ablation. The results obtained accurately represent the phenomena occurring in the porous liver tissue during the MW ablation. The SAR, temperature, and blood velocity profiles have a slightly different for various tumor diameters. The tumor porosity has only a small effect on the temperature distribution, but a clear effect on the blood velocity distribution. In addition, greater input MW power leads to a higher SAR value, thereby increasing the temperature and resulting in higher blood velocity within the porous liver tissue. The temperature profiles of the bioheat and porous media models are very similar at a particular time, but differ slightly in magnitude because the blood flow in the void of the porous media model has a small effect. The present model is examined for advancing the transport phenomena in biomedical applications.

Acknowledgements

The authors would like to gratefully acknowledge the Thailand Research Fund under the project no. TRG5780208, RTA598009 and Mahidol University for supporting this research.

Declaration of conflicting interests

The author(s) declared no potential conflicts of interest with respect to the research, authorship, and/or publication of this article.

Funding

The author(s) disclosed receipt of the following financial support for the research, authorship, and/or publication of this article: This research received the financial support from the Thailand Research Fund and Mahidol University.

References

1. Garrean S, Hering J, Saied A, et al. Ultrasound monitoring of a novel microwave ablation (MWA) device in porcine liver: lessons learned and phenomena observed on ablative effects near major intrahepatic vessels. *J Gastrointest Surg* 2009; 13: 334–340.
2. Haemmerich D, Santos ID, Schutt DJ, et al. In vitro measurements of temperature-dependent specific heat of liver tissue. *Med Eng Phys* 2006; 28: 194–197.
3. Hines-Peralta AU, Pirani N, Clegg P, et al. Microwave ablation: results with a 2.45-GHz applicator in ex vivo bovine and in vivo porcine liver. *Radiology* 2006; 239: 94–102.
4. Yang D, Converse MC, Mahvi DM, et al. Measurement and analysis of tissue temperature during microwave liver ablation. *IEEE Trans Biomed Eng* 2007; 54: 150–155.
5. Pennes HH. Analysis of tissue and arterial blood temperatures in the resting human forearm. *J Appl Physiol* 1998; 85: 5–34.
6. Gupta PK, Singh J and Rai KN. Numerical simulation for heat transfer in tissues during thermal therapy. *J Therm Biol* 2010; 35: 295–301.
7. Choi SY, Kwak BK and Seo T. Mathematical modeling of radiofrequency ablation for varicose veins. *Comput Math Method M* 2014; 2014: 485353.
8. Wu X, Liu B and Xu B. Theoretical evaluation of high frequency microwave ablation applied in cancer therapy. *Appl Therm Eng* 2016; 107: 501–507.
9. Shih TC, Yuan P, Lin WL, et al. Analytical analysis of the Pennes bioheat transfer equation with sinusoidal heat flux condition on skin surface. *Med Eng Phys* 2007; 29: 946–953.
10. Becker S. Analytic one dimensional transient conduction into a living perfuse/non-perfuse two layer composite system. *Int J Heat Mass Tran* 2012; 48: 317–327.
11. Klinger H. Heat transfer in perfused biological tissue—I: general theory. *B Math Biol* 1974; 36: 403–415.
12. Yang D, Converse MC and Mahvi MD. Expanding the bioheat equation to include tissue internal water evaporation during heating. *IEEE Trans Biomed Eng* 2007; 54: 1382–1388.
13. Keangin P, Wessapan T and Rattanadecho P. Analysis of heat transfer in deformed liver cancer modeling treated using a microwave coaxial antenna. *Appl Therm Eng* 2011; 31: 3243–3254.
14. Liu KC, Wang CC and Cheng PJ. Nonlinear behavior of thermal lagging in laser-irradiated layered tissue. *Adv Mech Eng* 2013; 5: 1–6.
15. He ZZ and Liu J. An efficient parallel numerical modeling of bioheat transfer in realistic tissue structure. *Int J Heat Mass Tran* 2016; 95: 843–852.
16. Nakayama A and Kuwahara F. A general bioheat transfer model based on the theory of porous media. *Int J Heat Mass Tran* 2008; 51: 3190–3199.
17. Mahjoob S and Vafai K. Analytical characterization of heat transport through biological media incorporating hyperthermia treatment. *Int J Heat Mass Tran* 2009; 52: 1608–1618.

18. Wang K, Tavakkoli F, Wang S, et al. Analysis and analytical characterization of bioheat transfer during radiofrequency ablation. *J Biomech* 2015; 48: 930–940.
19. Khakpour M and Vafai K. A comprehensive analytical solution of macromolecular transport within an artery. *Int J Heat Mass Tran* 2008; 51: 2905–2913.
20. Rattanadecho P and Keangin P. Numerical study of heat transfer and blood flow in two-layered porous liver tissue during microwave ablation process using single and double slot antenna. *Int J Heat Mass Tran* 2013; 58: 457–470.
21. Chiang J, Birla S, Bedoya M, et al. Modeling and validation of microwave ablations with internal vaporization. *IEEE Trans Biomed Eng* 2015; 62: 657–663.
22. Vyas DCM, Kumar S and Srivastava A. Porous media based bio-heat transfer analysis on counter-current artery vein tissue phantoms: applications in photo thermal therapy. *Int J Heat Mass Tran* 2016; 99: 122–140.
23. Chaichanyut M and Tungjitkusolmun S. Microwave ablation using four-tine antenna: effects of blood flow velocity, vessel location, and total displacement on porous hepatic cancer tissue.*Comput Math Method M* 2016; 2016:4846738.
24. McGahan JP, Brock JM, Tesluk H, et al. Hepatic ablation with use of radio-frequency electrocautery in the animal model. *J Vasc Interv Radiol* 1992; 3: 291–297.
25. Saito K, Hayashi Y, Yoshimura H, et al. Heating characteristics of array applicator composed of two coaxial-slot antennas for microwave coagulation therapy. *IEEE T Microw Theory* 2000; 48: 1800–1806.
26. Bellomo C. A mathematical model of the immersion of a spherical tumor with a necrotic core into a nutrient bath. *Math Comput Model* 2006; 43: 779–786.
27. Phasukkit P, Tungjitkusolmun S and Sangworasil M. Finite-element analysis and in vitro experiments of placement configurations using triple antennas in microwave hepatic ablation. *IEEE Trans Biomed Eng* 2009; 56: 2564–2572.
28. Keangin P, Rattanadecho P and Wessapan T. An analysis of heat transfer in liver tissue during microwave ablation using single and double slot antenna. *Int Commun Heat Mass* 2011; 38: 757–766.
29. Bertram JM, Yang D and Converse MC. Antenna design for microwave hepatic ablation using an axisymmetric electromagnetic model. *Biomed Eng Online* 2006; 5: 15.
30. Kee RJ, Coltrin ME and Glarborg P. *Chemically reacting flow: theory and practice*. Hoboken, NJ: John Wiley & Sons, 2003.
31. Shafahi M and Vafai K. Human eye response to thermal disturbances. ASME: J Heat *Trans* 2011; 133: 011009.
32. Wessapan T and Rattanadecho P. Specific absorption rate and temperature increase in human eye subjected to electromagnetic fields at 900 MHz. *ASME: J Heat Trans* 2012; 134: 091101.
33. Brinkman HC. On the permeability of media consisting of closely packed porous particles. *Appl Sci Res* 1949; 1: 81–86.
34. Al-Amiri AM. Analysis of momentum and energy transfer in a lid-driven cavity filled with a porous medium. *Int J Heat Mass Tran* 2000; 43: 3513–3527.
35. Rabin Y and Shitzer A. A numerical solution of the multidimensional freezing problem during cryosurgery. *J Biomech Eng* 1998; 120: 32–37.
36. Absalan H, SalmanOgli A, Rostami R, et al. Simulation and investigation of quantum dot effects as internal heat-generator source in breast tumor site. *J Therm Biol* 2012; 37: 490–495.
37. Chen ZP, Miller WH, Roemer RB, et al. Errors between two- and three-dimensional thermal model predictions of hyperthermia treatments. *Int J Hyperthermia* 1990; 6: 175–191.
38. Stauffer PR, Rossetto F, Prakash M, et al. Phantom and animal tissues for modelling the electrical properties of human liver. *Int J Hyperthermia* 2003; 19: 89–101.
39. Wessapan T, Srisawatdhisukul S and Rattanadecho P. The effects of dielectric shield on specific absorption rate and heat transfer in the human body exposed to leakage microwave energy. *Int Commun Heat Mass* 2011; 38: 255–262.
40. Deshazer G, Prakash P, Merck D, et al. Experimental measurement of microwave ablation heating pattern and comparison to computer simulations. *Int J Hyperthermia* 2017; 33: 74–82.